

Supporting Information

Ferrocene-Crosslinked Polypyrrole Hydrogel Derived Fe-N-doped Hierarchical Porous Carbon as Efficient Electrocatalysts for pH Universal ORR and Zn-air battery

Peng Sun,^{†a} Teng Zhang,^{†a} Haotian Luo,^a Jinli Dou,^a Weiwei Bian,^a Zhengxuan Pan,^a

Aili Zheng,^{*a} Baolong Zhou^{* a,b}

^a*School of Pharmacy, Weifang Medical University, Weifang, 261053, Shandong, P. R. China.*

^b*Shandong Engineering Research Center for Smart Materials and Regenerative Medicine, Weifang Medical University, Weifang, 261053, Shandong, P. R. China.*

E-mail: zhoubaolong@wfmc.edu.cn; zhengaili07@wfmc.edu.cn

[†]These authors contribute equal to this article.

Contents

Section 1. Materials and Characterization

Section 2. Experimental Details

Section 3. Electrochemical Measurements

Section 4. FTIR

Section 5. TG.

Section 6. Electrochemical Performance in Alkaline Media

Section 7. Electrochemical Performance in Neutral Media

Section 8. Electrochemical Performance in Acidic Media

Section 9. Supporting Tables

Section 10. Supporting References

Section 1. Materials and Characterization

Materials

1,1'-Ferrocenedicarboxylic Acid, Sodium hydroxide, Ammonium persulfate, pyrrole and isopropanol were purchased from commercial suppliers and used as received. Other chemicals and reagents were also purchased from commercial suppliers without further purification unless otherwise stated.

Characterization

Fourier Transform Infrared Spectroscopy (FTIR) was performed on KBr pellets in the range from 4000 to 400 cm^{-1} using Spectrum Spotlingt 400. Thermogravimetric analysis (TGA) were recorded using NETZSCH STA 449C analyzer from 25 °C to 900 °C at a heating rate of 10 °C min^{-1} under the protection of N_2 . The morphologies of powder samples were evaluated by field-emission scanning electron Microscopy (FESEM, Ultra 55) and transmission electron microscopy (TEM, Tecnai G2 20 TWIN) via dipping the prepared samples on a Cu-net. The adsorption and desorption measurements for N_2 were performed on a Belsorp max analyzer (Japan) at low temperature of 77 K. The specific surface areas were calculated using the BET model over a relative pressure (P/P_0) range of 0.05-0.15. Total pore volumes were calculated from the uptake at a relative pressure of 0.995. Before test, all these samples were degassed overnight under high vacuum at the temperature of 300 °C to remove the solvent or the water absorbed in the porous skeleton. X-ray Photoelectron Spectroscopy (XPS) was conducted on XPESCALAB 250Xi analyser. X-ray diffraction (XRD)

parameters were obtained using a Rigaku-DMAX 2500 diffractometer at a rate of 5° min^{-1} from 5° to 80° .

Section 2. Experimental Details

Synthesis of PF-xerogel

In a typical synthesis, 4.2 mL pyrrole was initially dissolved in 50 mL isopropanol. Then, 1,1'-Ferrocenedicarboxylic acid (1.053 g, 1.1 mmol), NaOH (0.27 g, 6.75 mmol) and ammonium persulfate (13.7 g, 61 mmol) that pre-dissolved in 100 mL H_2O were quickly mixed with pyrrole at the temperature of 4°C to give the FP hydrogel. The hydrogel was washed by ethanol and water thoroughly, and then subjected to freeze-drying to afford the PF-xerogels.^{S1}

Synthesis of PF-X

PF-X was prepared via direct carbonization of PF-xerogel directly under the Ar. Briefly, after finely grinding, PF-xerogel was loaded on a porcelain boat and then transferred into a tube furnace. Then, the pyrolysis was conducted under the atmosphere of Ar and heated to the target temperature ($X = 700, 800$ and 900°C) for 2 h. The target product, namely PF-X, is obtained after natural cooling to room temperature.

Section 3. Electrochemical Measurements

All electrochemical tests were performed at room temperature using standard three-chamber cells to record the electrode pairs of platinum grid, and the Ag/AgCl electrode was extremely saturated with KCl. All the potentials were referenced to the reversible hydrogen electrode (RHE) scale according to the

Nernst equation, *i. e.*, $E \text{ (RHE)} = E \text{ (Ag/AgCl)} + 0.059 \times \text{pH} + 0.197 \text{ V}$, at 25°C.

The working electrode can be either a rotating disk electrode (RDE) composed of a glass carbon disk (diameter 5.0mm) or a rotating ring disk electrode (RRDE) composed of a glass carbon disk (diameter 3 mm) surrounding an outer platinum ring (inner diameter 5 mm, outer diameter 7 mm). The catalyst ink is loaded on the working electrode surface. The catalyst inks and commercially available Pt/C (20 wt%) inks are made by dispersing 5.0 mg of the fresh-prepared catalyst or commercially available Pt/C (20 wt%) in an ultrasonic bath to a 500 μL solvent mixture (25 μL Naffion solution (5 wt%), 75 μL H_2O , and 400 μL ethanol) to a uniform suspension. The catalyst ink (8 μL) was dropped onto the surface of RDE or RRDE and dried in the air at room temperature.

The catalytic activity of the catalyst was measured by cyclic voltammetry (CV) and rotary disk electrode (RDE) at CHI-760 electrochemical station. All tests were carried out under alkaline (0.1 M KOH), neutral (0.1 PBS), or acidic conditions (0.1m HClO_4). CV was measured at 50 mV s^{-1} in various electrolytes saturated with O_2 or Ar. The RDE/RRDE tests were examined with a scanning rate of 5 mV s^{-1} at different speeds ranging from 400 to 2500 rpm. The K-L equation was applied to investigate the ORR kinetic parameters. The K-L equation can be described as follows^{S2}:

$$\frac{1}{J} = \frac{1}{J_L} + \frac{1}{J_K} = \frac{1}{B \omega^{1/2}} + \frac{1}{J_K} \quad (1)$$

Where J is the current density, J_L is the current that was measured; J_K

represents the kinetic-limiting current and ω is the rotation speeds of electrode.

$$B = 0.62nFC_0(D_0)^{2/3}V^{-1/6} \quad (2)$$

In equation 2, n is the total number of transferred electrons during the oxygen reduction process; F is Faradaic constant ($F = 96485 \text{ C mol}^{-1}$), C_0 is the O_2 concentration (solubility) in 0.1 M KOH electrolyte ($1.2 \times 10^{-6} \text{ mol cm}^{-3}$); D_0 is the O_2 diffusion coefficient ($1.90 \times 10^{-5} \text{ cm}^2 \text{ s}^{-1}$), and V is the kinematic viscosity of the O_2 saturated 0.1 M KOH solution ($0.01 \text{ cm}^2 \text{ s}^{-1}$). For the RRDE measurements, the disk electrode was also scanned with a rate of 5 mV s^{-1} at a constant ring potential of 1.5 V vs. RHE . The peroxide percentage (H_2O_2 yields) and the transferred number of electron (n) were calculated according to the following equations (3) - (4):^{S3}

$$\text{H}_2\text{O}_2\% = \frac{I_r/N}{200I_d + I_r/N} \quad (3)$$

$$N = 4 \frac{I_d}{I_d + I_r/N} \quad (4)$$

In equation 3 and 4, I_d is the disk current, and I_r refers to the ring current and N represents the current collection efficiency of the Pt ring ($N=0.4581$).

Section 4. FT-IR Spectra

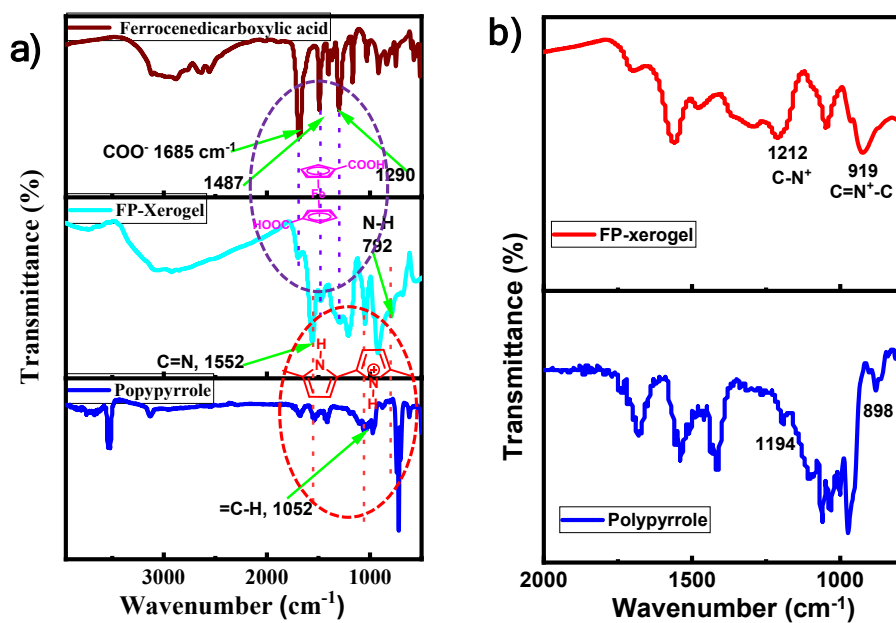


Figure S1. FTIR spectra of polypyrrole, ferrocene-dicarboxylic acid together with final PF-xerogel.

Section 5. TG

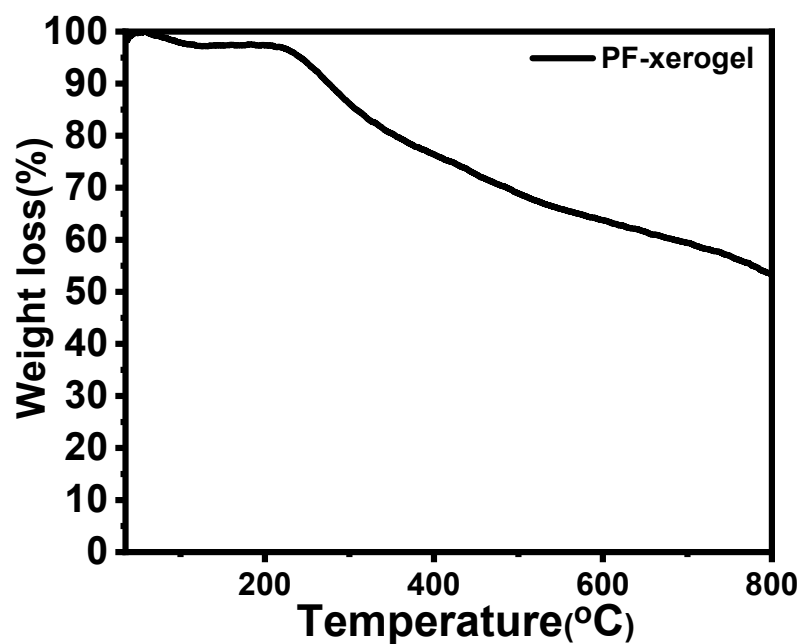


Figure S2. TG of prepared polymers.

Section 6. Electrochemical Performance in Alkaline Conditions

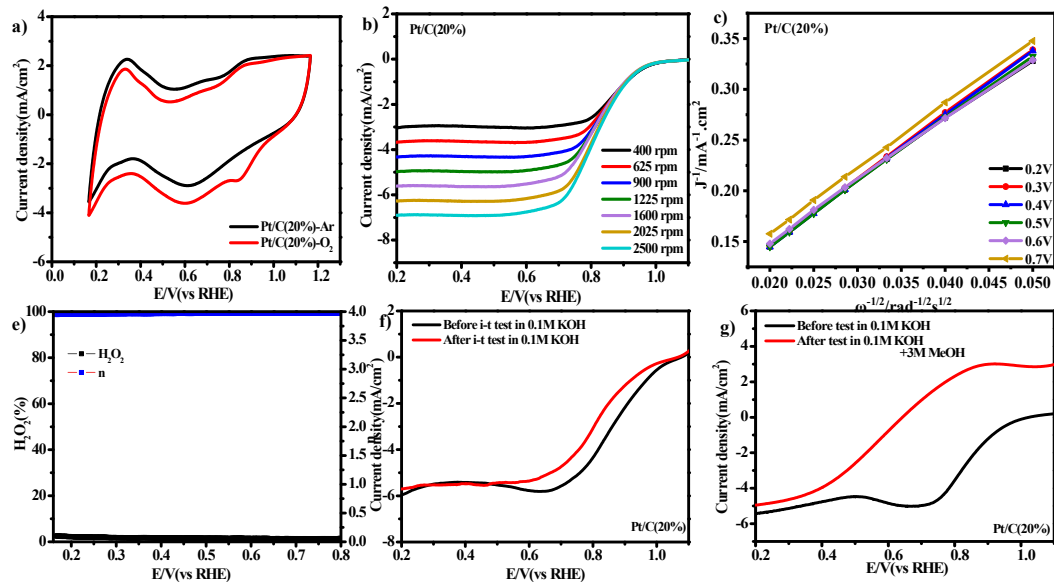


Figure S3. a) CV curves of commercial Pt/C (20%) on a glassy carbon electrodes in 0.1 M KOH saturated with O₂ or Ar at a sweep rate of 50 mV s⁻¹; b) LSV of commercial Pt/C (20%) at various rotation speeds; c) K-L plots curves of commercial Pt/C (20%); e) Percentage of hydrogen peroxide yield and the electron transfer number (n) of Pt/C at different potentials; f) Polarization curves of Pt/C (20%) measured by RDE in O₂-saturated 0.1 M KOH before (red

line) and after (black line) the i-t (20000 s) experiments; g) LSV curve of Pt/C measured before and after the injection of 3 M methanol.

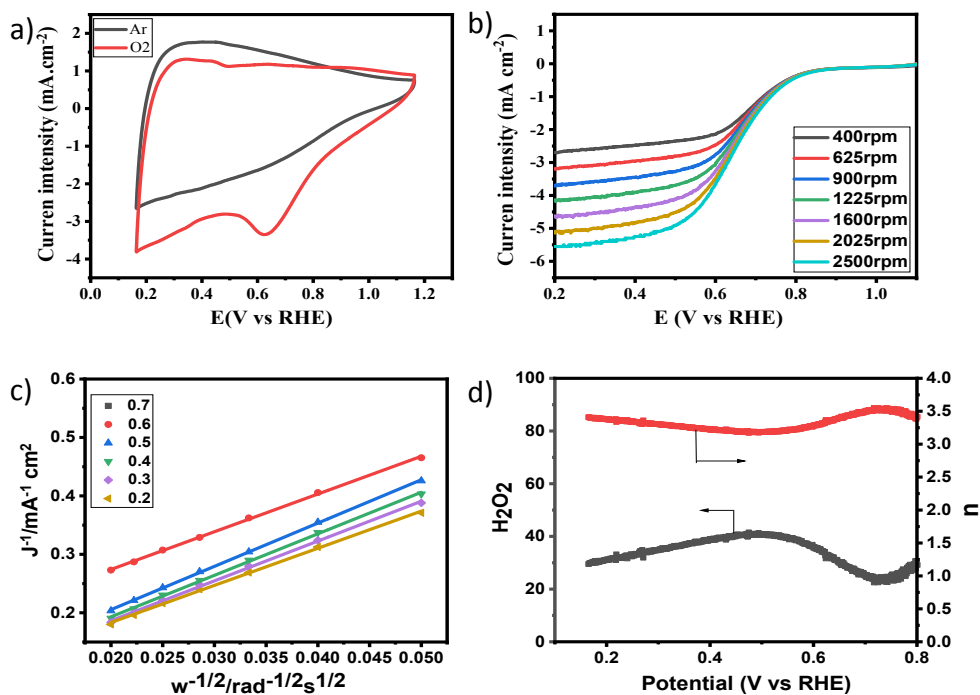


Figure S4. Electrochemical performance of PF-700 in 0.1 M KOH. a) CV curves PF-700 on glassy carbon electrodes in 0.1 M KOH saturated with O₂ or argon at a sweep rate of 50 mV s⁻¹. b) LSV of commercial PF-700 at different rotation speeds; c) K-L plots curves of PF-700 at different potentials; d) Percentage of hydrogen peroxide yield and the electron transfer number (n) of PF-700 at different potentials.

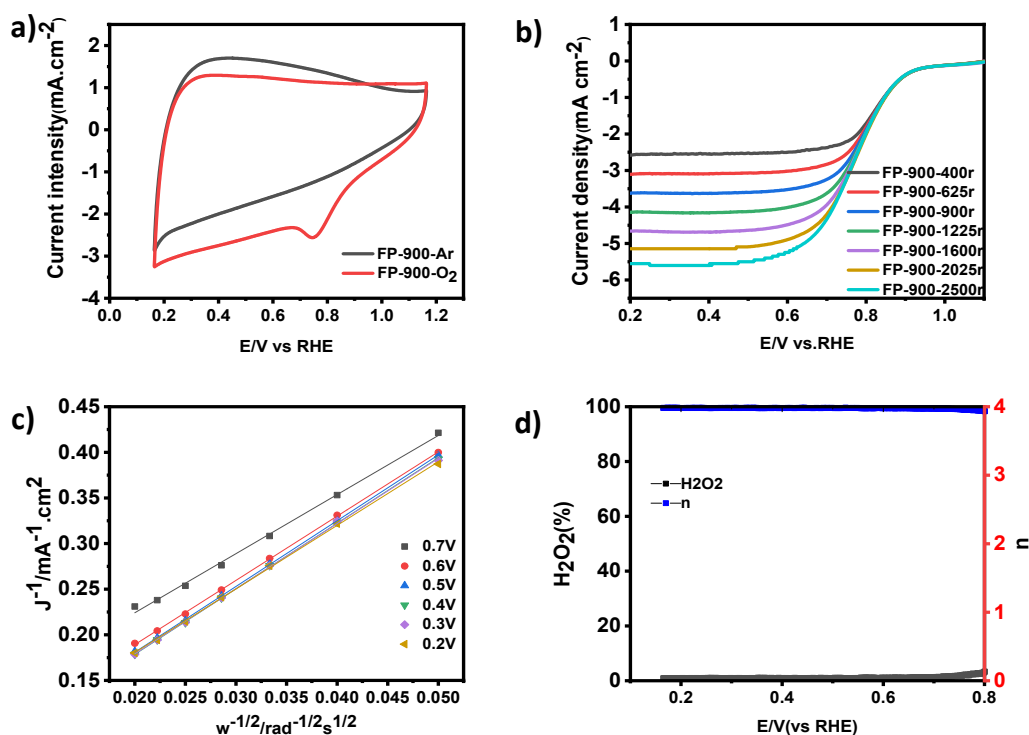


Figure S5. Electrochemical performance of PF-900 in 0.1 M KOH. a) CV curves PF-900 on glassy carbon electrodes in 0.1 M KOH saturated with O₂ or argon at a sweep rate of 50 mV s⁻¹. b) LSV of commercial PF-900 at different rotation speeds; c) K-L plots curves of PF-900 at different potentials; d) Percentage of hydrogen peroxide yield and the electron transfer number (n) of PF-900 at different potentials.

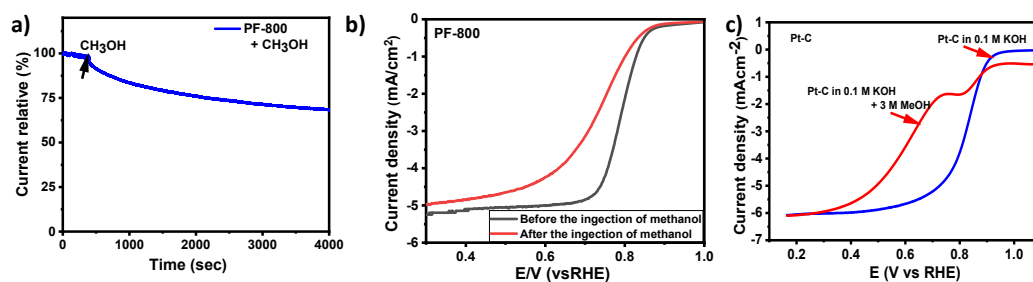


Figure S6. a) Methanol immunity test of PF-800 in which the methanol was injected at the 400 s. b) LSV curve of PF-800 measured before and after the injection of 3 M methanol; c) LSV curve of PF-800 measured before and after the injection of 3 M methanol.

Section 7. Electrochemical Performance in Neutral Media

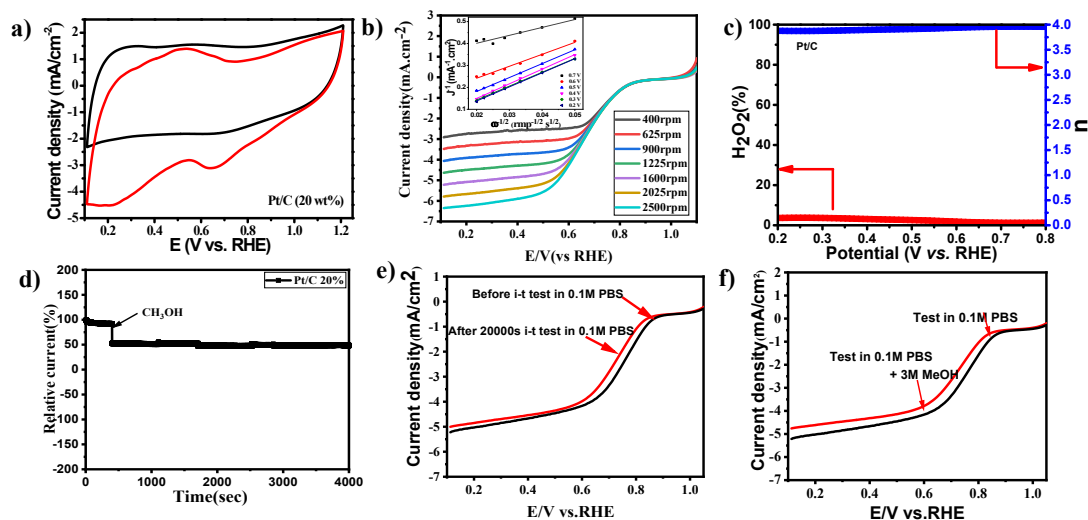


Figure S7. Electrochemical performance of Pt/C measured in neutral conditions. a) CV curves of commercial Pt/C (20%) on glassy carbon electrodes in water solution of 0.1 M PBS saturated with O₂ or argon at a sweep rate of 50 mV s⁻¹. b) LSV of commercial Pt/C (20%) at different rotation speeds, the insert part is the K-L plots fitting curves of Pt/C (20%) at different potentials; c) Percentage of hydrogen peroxide yield and the electron transfer number (n) of Pt/C (20%) at different potentials; d) Chronoamperometric response of commercial Pt/C at around E_{1/2} in O₂-saturated PBS at 1600 rpm and the methanol was added at 400s; e) Polarization curves of Pt/C (20%) measured by RDE in O₂-saturated 0.1 M PBS before (red line) and after (black line) the i-t (20000 s) experiments; f) LSV curve of Pt/C (20%) measured before and after the injection of 3 M methanol.

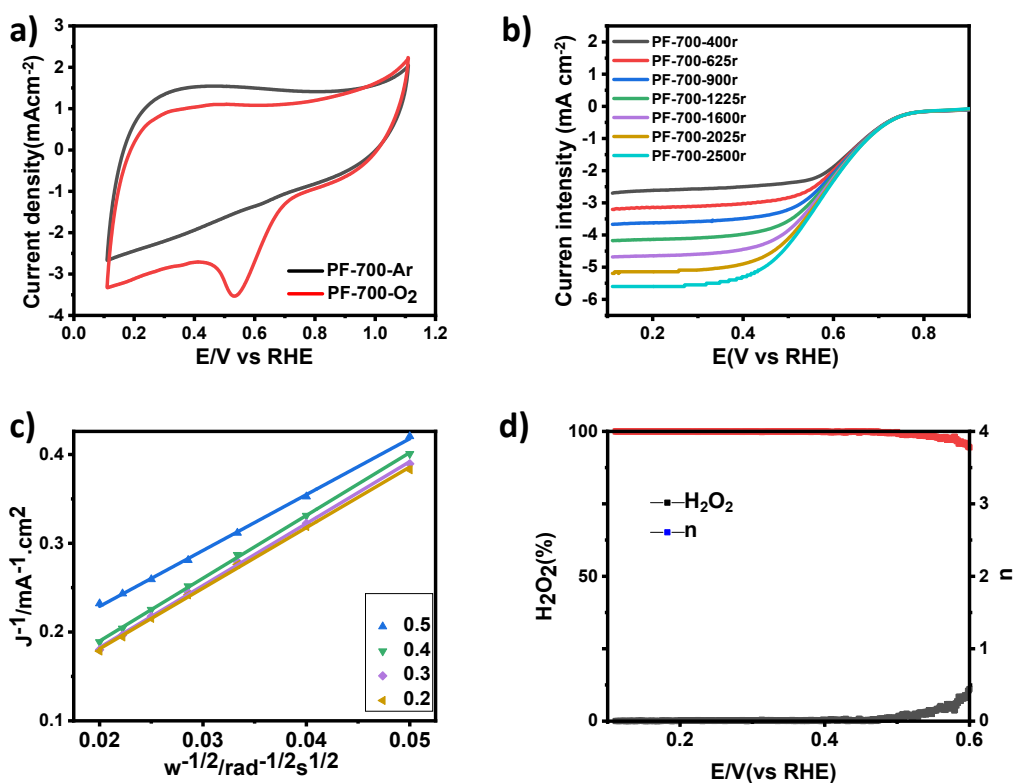


Figure S8. Electrochemical performance of PF-700 in 0.1 M PBS. a) CV curves PF-700 on glassy carbon electrodes in 0.1 M PBS saturated with O₂ or argon at a sweep rate of 50 mV s⁻¹; b) LSV of commercial PF-700 at different rotation speeds; c) K-L plots curves of PF-700 at different potentials; d) Percentage of hydrogen peroxide yield and the electron transfer number (n) of PF-700 at different potentials.

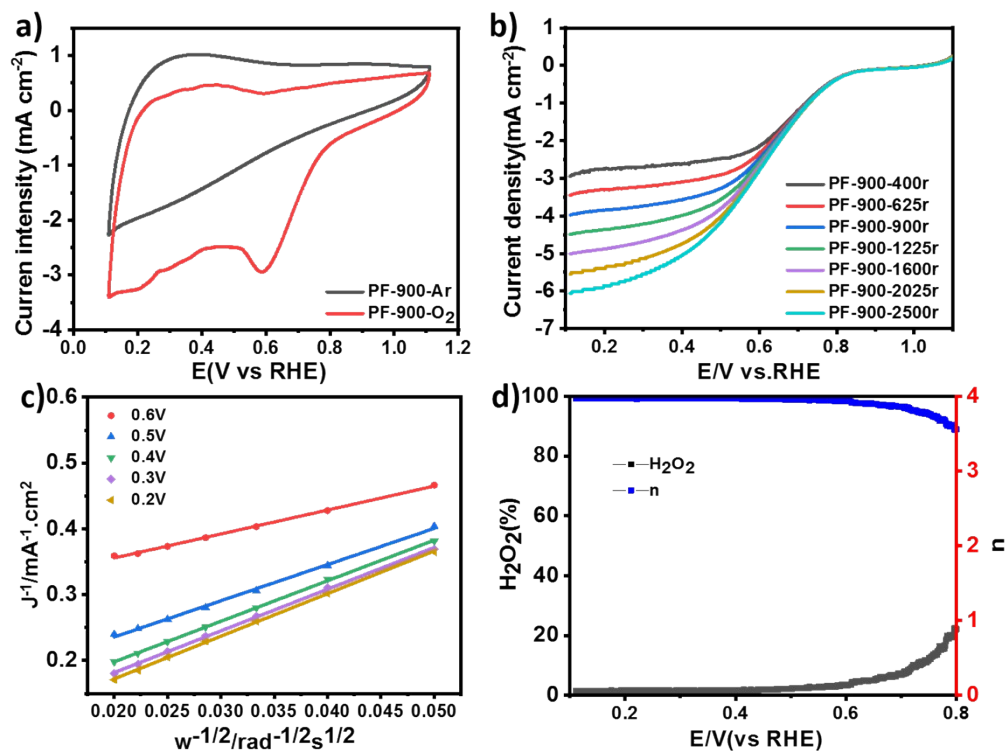


Figure S9. Electrochemical performance of PF-900 in 0.1 M PBS. a) CV curves PF-900 on glassy carbon electrodes in 0.1 M PBS saturated with O_2 or argon at a sweep rate of 50 mV s^{-1} . b) LSV of commercial PF-900 at different rotation speeds; c) K-L plots curves of PF-900 at different potentials; d) Percentage of hydrogen peroxide yield and the electron transfer number (n) of PF-900 at different potentials.

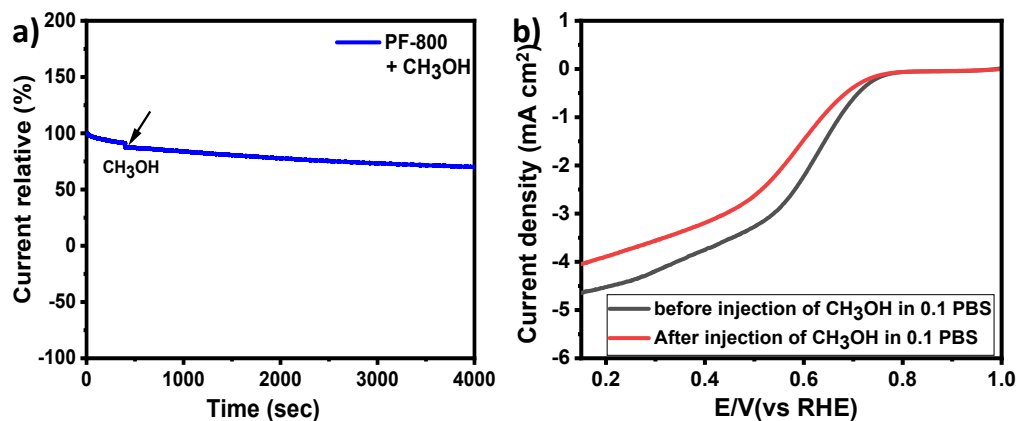


Figure S10. a) Methanol immunity test of PF-800 in which the methanol was injected at the 400 s. b) LSV curve of PF-800 measured before and after the injection of 3 M methanol.

Section 8. Electrochemical Performance in Acidic Media

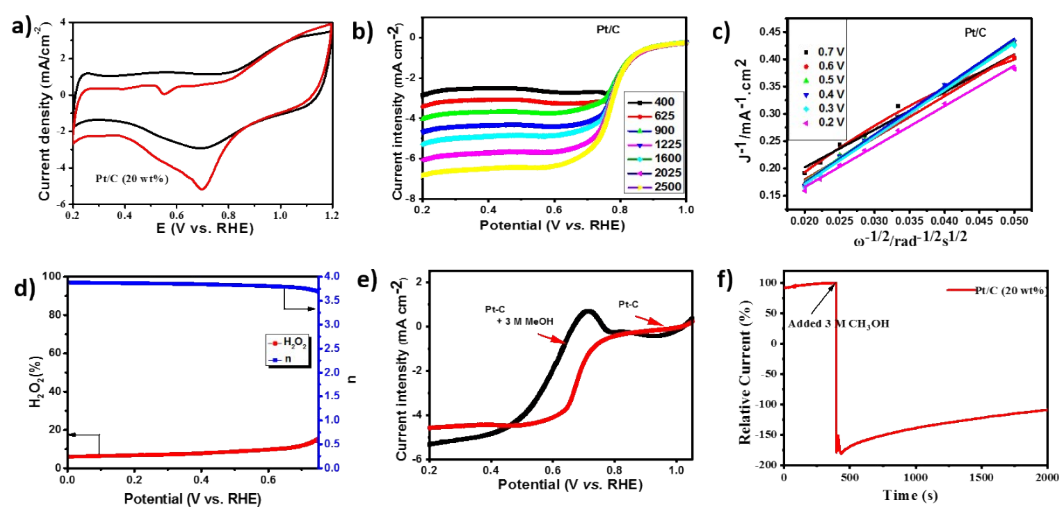


Figure S11. Electrochemical performance of commercial Pt/C in acidic conditions: a) CV curves of commercial Pt/C (20%) on glassy carbon electrodes in water solution of 0.1 M HClO₄ saturated with O₂ or argon at a sweep rate of 50 mV s⁻¹. b) LSV of commercial Pt/C (20%) at different rotation speeds; c) K-L plots curves of Pt/C (20%) at different potentials; d) Percentage of hydrogen peroxide yield and the electron transfer number (n) of Pt/C (20%) at different potentials; e) Polarization curves of Pt/C (20%) measured by RDE in O₂-saturated 0.1 M HClO₄ before (red line) and after (black line) the injection of 3 M methanol; f) i-t response of Pt/C (20%) before and after the injection of methanol.

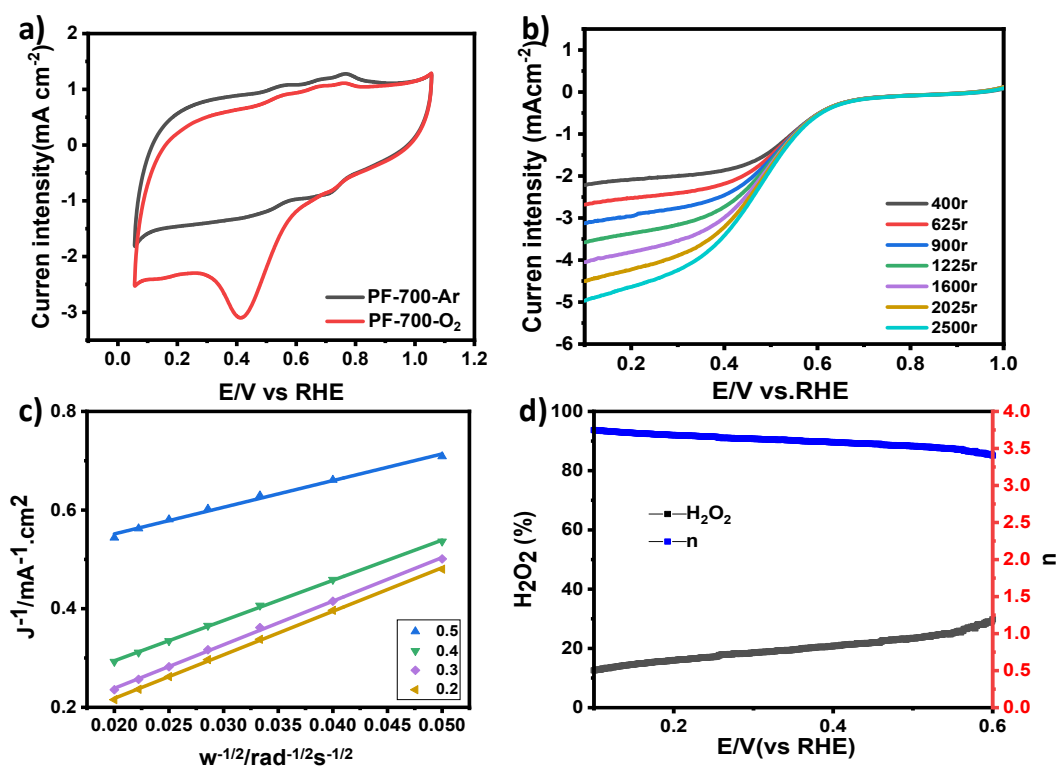


Figure S12. Electrochemical performance of PF-700 in 0.1 M HClO₄. a) CV curves PF-700 on glassy carbon electrodes in 0.1 M HClO₄ saturated with O₂ or argon at a sweep rate of 50 mV s⁻¹. b) LSV of commercial PF-700 at different rotation speeds; c) K-L plots curves of PF-700 at different potentials; d) Percentage of hydrogen peroxide yield and the electron transfer number (n) of PF-700 at different potentials.

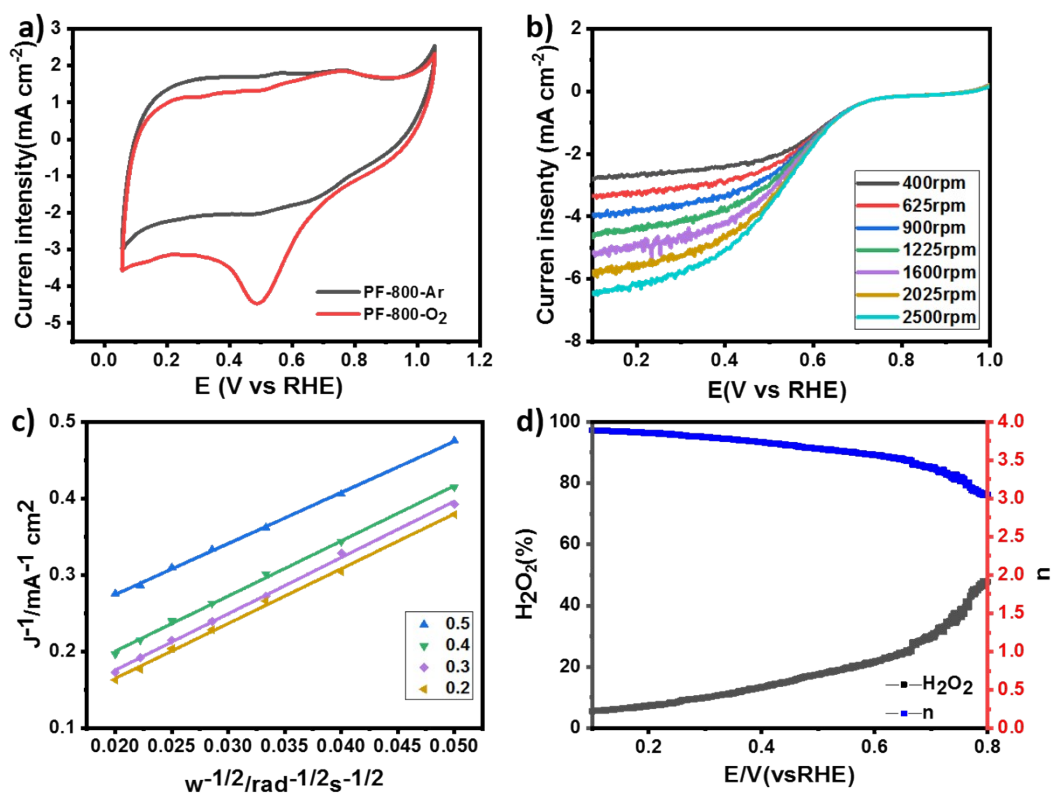


Figure S13. Electrochemical performance of PF-900 in 0.1 M HClO₄. a) CV curves PF-900 on glassy carbon electrodes in 0.1 M HClO₄ saturated with O₂ or argon at a sweep rate of 50 mV s⁻¹. b) LSV of commercial PF-700 at different rotation speeds; c) K-L plots curves of PF-900 at different potentials; d) Percentage of hydrogen peroxide yield and the electron transfer number (n) of PF-900 at different potentials.

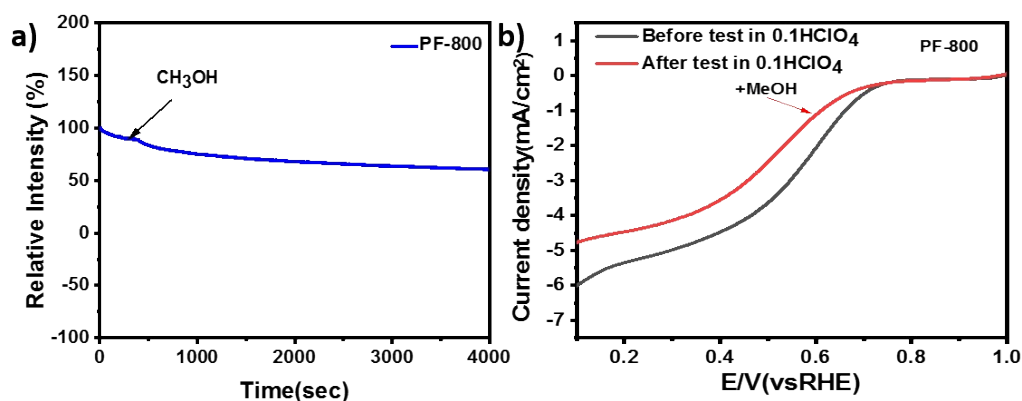


Figure S14. a) Methanol immunity test of PF-800 in acidic media in which the methanol was injected at the 400 s. b) LSV curve of PF-800 measured before and after the injection of 3 M methanol.

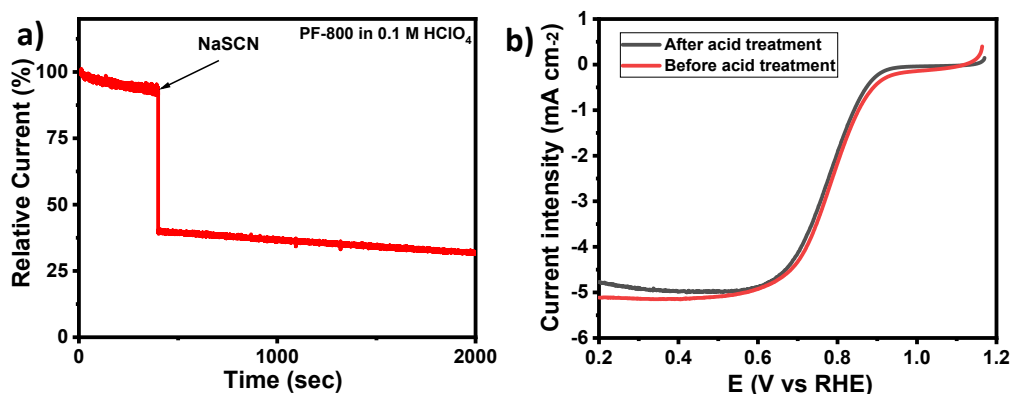


Figure S15. a) Current-time (I-t) curves of PF-800 in O₂-saturated 0.1 M HClO₄ solution without and with SCN⁻; (b) RDE results of PF-800 and PF-800 treated with HCl in O₂-saturated 0.1 M KOH solution on a rotating disk electrode (1600 rpm) with a scan rate of 5 mV s⁻¹.

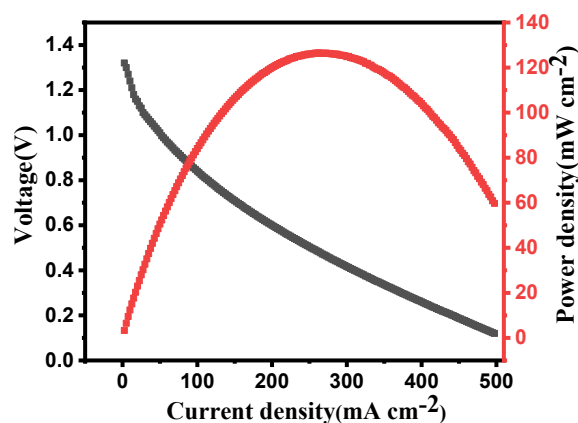


Figure S16. Polarization curve and the corresponding power density curves of the Zn-air battery based on the PF-800.

Section 9. Supporting Tables

Table S1. Main parameters of the prepared catalysts combined with the commercial Pt/C catalysts in alkaline conditions

Sample	On-set Potential (E _{onset} , V)	Half-wave potential (E _{1/2} , V)	Limited Current density (mA cm ⁻²)	Electron transfer number (n, at 0.5 V)
PF-700	0.86	0.65	4.65	3.20
PF-800	0.96	0.79	5.16	3.75
PF-900	0.92	0.78	4.81	3.93
Pt/C(20%)	1.02	0.82	5.51	3.97

Table S2. Main parameters of the prepared catalysts combined with the commercial Pt/C catalysts in neutral conditions

Sample	On-set Potential (E _{onset} , V)	Half-wave potential (E _{1/2} , V)	Current density (mA cm ⁻² ; at 0.1V)	Electron transfer number (n, at 0.1 V)
PF-700	0.80	0.59	4.62	3.20
PF-800	0.89	0.65	4.79	3.75
PF-900	0.85	0.61	5.00	3.93
Pt/C (20%)	0.96	0.68	5.56	3.97

Table S3. Main parameters of the prepared catalysts combined with the commercial Pt/C catalysts in acidic conditions

Sample	On-set Potential (E _{onset} , V)	Half-wave potential (E _{1/2} , V)	Current density (mA cm ⁻² ; at 0.1V)	Electron transfer number (n, at 0.5 V)
PF-700	0.72	0.51	1.06	3.89
PF-800	0.80	0.61	1.66	3.86
PF-900	0.77	0.54	3.62	3.92
Pt/C(20%)	0.93	0.80	5.20	3.94

Table S4. Comparison of zinc-air battery utilizing PF-800 with other Fe-based electrocatalysts reported recently.

Catalysts	E _{1/2} (V vs RHE)	Power density (mW cm ⁻²)	specific capacity (mAh g _{Zn} ⁻¹)	Stability
PF-800 (This work)	0.79	131	748	80.3 h@10 mA cm ⁻²
FeNi-NC ^[4]	0.83	80.8	/	23 h@5 mA cm ⁻²
S,N-Fe/N/CCNT ^[5]	0.85	102.7	/	100h@5 mA cm ⁻²
h-FeNC ^[6]	0.84	215	/	/
Co ₂ P@am-FePO ₄ ^[7]	0.86	152	852.36	/
Fe-NC-900-M ^[8]	0.88	271	/	/
HFCP-850 ^[9]	0.78	/	820	90.8h@10 mA cm ⁻²
3D-Fe/N-G#4 ^[10]	0.85	168.2	/	60h@10 mA cm ⁻²
NiFe@NCx ^[11]	0.86	85	/	108 h@10 mA cm ⁻²
N-Fc-800 ^[12]	0.82	178	/	16h@10 mA cm ⁻²
FC-950 ^[13]	0.83	176.8	/	/

Section 10. Supporting References

[1] J. Yang, X. Wang, B. Li, L. Ma, L. Shi, Y. Xiong, and H. Xu., *Adv. Funct. Mater.* **2017**, 1606497.

[2] H. Yunhu, Y. Wang, W. Chen, R. Xu, L. Zheng, J. Zhang, J. Luo, R. Shen, Y. Zhu, W. Cheong, C.

Chen, Q. Peng, D. Wang, and Y. Li, *J. Am. Chem. Soc.* **2017**, 139, 17269-17272.

- [3] L. Yang, J. Shui, L. Du, Y. Shao, J. Liu, L. Dai, Z. Hu, *Adv. Mat.* **2019**, 31, 1804799.
- [4] L. Yang, X. Zeng, D. Wang, D. Cao, *Energy Storage Mater.* **2018**, 2, 277-283.
- [5] P. Chen, T. Zhou, L. Xing, K. Xu, Y. Tong, H. Xie, L. Zhang, W. Yan, W. Chu, C. Wu, *Angew. Chem., Int. Ed.* **2017**, 129, 625-629.
- [6] R. Dun, M. Hao, Y. Su, and W. Li, *J. Mater. Chem. A*, **2019**, 7, 12518-12525.
- [7] D. Cheng, Z. Wang, C. Chen, and K. Zhou, *Chem. Mater.* **2019**, 31, 8026-8034.
- [8] Z. Liu, J. Liu, H. Wu, G. Shen, Z. Le, G. Chen, and Y. Lu, *Nanoscale*, **2018**, 10, 16996-17001.
- [9] J. Dou, M. Qi, H. Wang, W. Shi, X. Luan, W. Guo, L. Xiao, C. Zhao, D. Cheng, T. Jiang, W. Zhang, Zhang, W. Bian, B. Zhou, *Micropor. Mesopor. Mater.* 2021, DOI: 10.1016/j.micromeso.2021.111101.
- [10] C. Wang, Z. Li, L. Wang, X. Niu, S. Wang, *ACS Sustainable Chem. Eng.*, **2019**, 7, 13873-13885.
- [11] J. Zhu, M. Xiao, Y. Zhang, Z. Jin, Z. Peng, C. Liu, S. Chen, J. Ge, W. Xing, *ACS Catal.*, 2016, 6, 6335-6342.
- [12] B. Zhou, L. Liu, P. Cai, G. Zeng, X. Li, Z. Wen and L. Chen, *J. Mater. Chem. A*, 2017, 5, 22163.
- [13] X. Liu, X. Liang, H. Lou, H. Wang, H. Li, S.n Zhang, S. Zhu, W. Han, and B. Zhou, *Sustainable Energy Fuels*, 2021, 5, 1067-1074.